Extending the Spectral Difference Method with Divergence Cleaning (SDDC) to the Hall MHD Equations

Russell J. Hankey[1*], Kuangxu Chen[1] and Chunlei Liang[1]

[1] Clarkson University, Potsdam, New York, 13699

[*] hankeyrj@clarkson.edu

Abstract

The Hall Magnetohydrodynamic (MHD) equations are an extension of the standard MHD equations that include the "Hall" term from the general Ohm's law. The Hall term decouples ion and electron motion physically on the ion inertial length scales. Implementing the Hall MHD equations in a numerical solver allows more physical simulations for plasma dynamics on length scales less than the ion inertial scale length but greater than the electron inertial length. The present effort is an important step towards producing physically correct results to important problems, such as the Geospace Environmental Modeling (GEM) Magnetic Reconnection problem. The solver that is being modified is currently capable of solving the resistive MHD equations on unstructured grids using the spectral difference scheme which is an arbitrarily high-order method that is relatively simple to parallelize. The GEM Magnetic Reconnection problem is used to evaluate whether the Hall MHD equations have been correctly implemented in the solver using the spectral difference method with divergence cleaning (SDDC) algorithm by comparing against the reconnection rates reported in the literature.

1 Introduction

Accurate simulations of magnetohydrodynamics problems rely on the ability to control the divergence error of the magnetic field $\nabla \cdot \mathbf{B}$ [1, 5, 13]. The constrained transport method [11] inherently satisfies the divergence-free condition $\nabla \cdot \mathbf{B} = 0$, making it an attractive solution. The high-order spectral difference (SD) method was built using the constrained transport framework [6], though unstructured grids are not supported in order to keep the stencil compact. Instead of satisfying the divergence free condition exactly, other methods can be used, including the projection method [16], the eight-wave formulation method [12], the hyperbolic divergence

cleaning (DC) method [9], and the locally divergence-free discontinuous Galerkin (DG) method [8]. The DC method is commonly used because of its simplicity, robustness, and flexibility to unstructured grids. The DC method adds a generalized Lagrange multiplier (GLM) and assumes $\nabla \cdot \mathbf{B}$ will not equal zero to couple the divergence-free condition with the original MHD equations.

The implementation of divergence cleaning to the spectral difference method (SDDC) has been accomplished for the resistive MHD equations [7]. However, more accurate simulations are expected to be produced when using the Hall MHD equations instead of the resistive MHD equations [15]. The Hall MHD equations are derived using the same process as the resistive MHD equations when the Hall term is no longer neglected in the general Ohm's Law [14].

2 Governing Equations

2.1 Hall MHD Equations

The compressible Hall MHD equations [14] are a set of nonlinear hyperbolic equations,

$$\frac{\partial \mathbf{Q}}{\partial t} + \nabla \cdot \mathbf{F} = \mathbf{0}, \tag{1}$$

where $\mathbf{Q} = (\rho, \rho\mathbf{U}, e, \mathbf{B})^{\mathbf{T}}$ is the vector of conserved variables, with ρ as the density, $\mathbf{U} = (u, v, w)^{\mathbf{T}}$ as the velocity vector, e as the total energy, and $\mathbf{B} = (B_x, B_y, B_z)^{\mathbf{T}}$ as the magnetic field. The total flux $\mathbf{F} = \mathbf{F}_{inv} - \mathbf{F}_{vis}$ consists of the inviscid fluxes minus the viscous fluxes. The inviscid flux vector is

$$\mathbf{F}_{inv}(\mathbf{Q}) = \begin{bmatrix} \rho\mathbf{U} \\ \rho\mathbf{U} \otimes \mathbf{U} + \left(p + \frac{1}{2}\|\mathbf{B}\|^2\right) \mathtt{I} - \mathbf{B} \otimes \mathbf{B} \\ \mathbf{U}\left(e + p + \frac{1}{2}\|\mathbf{B}\|^2\right) + \mathbf{U}_H\|\mathbf{B}\|^2 - \mathbf{B}((\mathbf{U} + \mathbf{U}_H) \cdot \mathbf{B}) \\ (\mathbf{U} + \mathbf{U}_H) \otimes \mathbf{B} - \mathbf{B} \otimes (\mathbf{U} + \mathbf{U}_H) \end{bmatrix}, \tag{2}$$

and the viscous flux vector is

$$\mathbf{F}_{vis}(\mathbf{Q}, \nabla\mathbf{Q}) = \begin{bmatrix} 0 \\ \tau \\ \tau \cdot \mathbf{U} - \mathbf{q} - \eta(\nabla \times \mathbf{B}) \times \mathbf{B} \\ \eta\left((\nabla\mathbf{B})^{\mathbf{T}} - \nabla\mathbf{B}\right) \end{bmatrix}, \tag{3}$$

where p is the hydrodynamic pressure; η is the magnetic resistivity; $\|\cdot\|$ is the Euclidean vector norm; $\mathbf{U}_H$ is the Hall velocity, defined as $\mathbf{U}_H = -\mathbf{J}/\rho$ where $\mathbf{J}$ is the current density; and $\mathtt{I}$ is the identity matrix. The total energy e is defined as

$$e = \frac{p}{\gamma - 1} + \frac{1}{2}\rho\|\mathbf{U}\|^2 + \frac{1}{2}\|\mathbf{B}\|^2, \tag{4}$$

where γ is the specific heat ratio for an ideal gas. The τ is the shear stress tensor,

$$\tau = \mu \left(\nabla \mathbf{U} + (\nabla \mathbf{U})^{\mathbf{T}} \right) + \lambda (\nabla \cdot \mathbf{U}) \mathtt{I}, \tag{5}$$

where μ is the dynamic viscosity, $\lambda = -2/3\mu$ based on the Stokes hypothesis. The heat flux vectors $\mathbf{q} = -\kappa \nabla \mathbf{T}$, where κ is the thermal conductivity. We use the ideal gas relation $p = \rho R T$ as the equation of state.

2.2 Divergence Cleaning

The GLM approach shown here is a modification proposed by Derigs in [10] and implemented by Chen & Liang (2022) in [7] for the resistive MHD equations. The DC method used in this paper modifies the approach taken in Chen & Liang (2022) [7] for the Hall MHD equations as follows

$$\begin{aligned} \frac{\partial}{\partial t} \begin{bmatrix} \rho \\ \rho \mathbf{U} \\ \epsilon \\ \mathbf{B} \\ \psi \end{bmatrix} + \nabla \cdot \begin{bmatrix} \rho \mathbf{U} \\ \rho \mathbf{U} \otimes \mathbf{U} + \left(p + \frac{1}{2} \|\mathbf{B}\|^2 \right) \mathtt{I} - \mathbf{B} \otimes \mathbf{B} \\ \mathbf{U} \left(e + p + \frac{1}{2} \|\mathbf{B}\|^2 \right) + \mathbf{U}_H \|\mathbf{B}\|^2 - \mathbf{B}((\mathbf{U} + \mathbf{U}_H) \cdot \mathbf{B}) + c_h \psi \mathbf{B} \\ (\mathbf{U} + \mathbf{U}_H) \otimes \mathbf{B} - \mathbf{B} \otimes (\mathbf{U} + \mathbf{U}_H) + c_h \psi \mathtt{I} \\ c_h \mathbf{B} \end{bmatrix} \\ = - \begin{bmatrix} 0 \\ (\nabla \cdot \mathbf{B}) \mathbf{B} \\ (\nabla \cdot \mathbf{B}) \mathbf{U} \cdot \mathbf{B} \\ (\nabla \cdot \mathbf{B}) \mathbf{U} \\ \alpha \psi \end{bmatrix}, \end{aligned} \tag{6}$$

with the augmented total energy ϵ defined as

$$\epsilon = e + \frac{1}{2} \psi^2 = \frac{p}{\gamma - 1} + \frac{1}{2} \rho \|\mathbf{U}\|^2 + \frac{1}{2} \|\mathbf{B}\|^2 + \frac{1}{2} \psi^2. \tag{7}$$

The new scalar ψ is an auxiliary transport variable that couples the divergence-free condition with the ideal MHD equations. The viscous fluxes are not modified with the inclusion of ψ. The hyperbolic DC speed c_h is

$$c_h = \sqrt{\lambda_{max} (\lambda_{max} - max_{\Omega}(|u|, |v|, |w|))}, \tag{8}$$

where λ_{max} denotes the largest characteristic speed of the Hall MHD system, which is the Whistler wave speed. The speed c_h is updated after the computation of numerical flux every iteration. The first four nonconservative source terms are the Powell source vector [12], allowing better control over the divergence-free condition. The last nonconservative term, $-\alpha\psi$, ensures that ψ decays exponentially in

the region where $\nabla \cdot \mathbf{B} \approx 0$, and $\alpha = 2$ is chosen. The inclusion of the Powell non-conservative term and a non-conservative GLM term in the energy equation is necessary for Galilean invariance [4]. The SD method for viscous resistive GLM - Hall MHD in 2D is created by rewriting Eqn. (6) as

$$\frac{\partial \mathbf{Q}}{\partial t} + \frac{\partial \mathbf{F}}{\partial x} + \frac{\partial \mathbf{G}}{\partial y} + \mathbf{M} = \mathbf{0}, \tag{9}$$

where $\mathbf{Q} = (\rho, \rho u, \rho v, \rho w, \epsilon, B_x, B_y, B_z, \psi)^{\mathbf{T}}$, and nonlinear fluxes are composed of inviscid, viscous and Hall parts,

$$\mathbf{F} = \mathbf{F}_{inv} - \mathbf{F}_{vis} + \mathbf{F}_{Hall}, \quad \mathbf{G} = \mathbf{G}_{inv} - \mathbf{G}_{vis} + \mathbf{G}_{Hall}. \tag{10}$$

The inviscid fluxes are

$$\begin{aligned}
\mathbf{F}_{inv}(\mathbf{Q}) = &\begin{bmatrix}
\rho u \\
\rho u^2 + p + \|\mathbf{B}\|^2/2 - B_x^2 \\
\rho uv - B_x B_y \\
\rho uw - B_x B_z \\
(\epsilon - \psi^2/2 + p + \|\mathbf{B}\|^2/2 - B_x^2)u - B_x(\mathbf{U}\cdot\mathbf{B}) + c_h \psi B_x \\
c_h \psi \\
(uB_y - vB_x) \\
-(wB_x - uB_z) \\
c_h B_x
\end{bmatrix}, \\
\mathbf{G}_{inv}(\mathbf{Q}) = &\begin{bmatrix}
\rho v \\
\rho uv - B_x B_y \\
\rho v^2 + p + \|\mathbf{B}\|^2/2 - B_y^2 \\
\rho vw - B_y B_z \\
(\epsilon - \psi^2/2 + p + \|\mathbf{B}\|^2/2 - B_y^2)v - B_y(\mathbf{U}\cdot\mathbf{B}) + c_h \psi B_y \\
-(uB_y - vB_x) \\
c_h \psi \\
(vB_z - wB_y) \\
c_h B_y
\end{bmatrix}.
\end{aligned} \tag{11}$$

The viscous fluxes are

$$\mathbf{F}_{vis}(\mathbf{Q},\nabla\mathbf{Q}) = \begin{bmatrix} 0 \\ \tau_{xx} \\ \tau_{yx} \\ \tau_{zx} \\ u\tau_{xx} + v\tau_{yx} + w\tau_{zx} + \kappa T_x + \nabla(B_y J_z - B_z J_y) \\ 0 \\ \eta J_z \\ -\eta J_y \\ 0 \end{bmatrix},$$

$$\mathbf{G}_{vis}(\mathbf{Q},\nabla\mathbf{Q}) = \begin{bmatrix} 0 \\ \tau_{xy} \\ \tau_{yy} \\ \tau_{zy} \\ u\tau_{xy} + v\tau_{yy} + w\tau_{zy} + \kappa T_y + \nabla(B_z J_x - B_x J_z) \\ -\eta J_z \\ 0 \\ \eta J_x \\ 0 \end{bmatrix}. \tag{12}$$

The Hall fluxes are

$$\mathbf{F}_{vis}(\mathbf{Q},\nabla\mathbf{Q}) = \begin{bmatrix} 0 \\ 0 \\ 0 \\ 0 \\ \|\mathbf{B}\|u_{Hall} - B_x(B_x u_{Hall} + B_y v_{Hall} + B_z w_{Hall}) \\ 0 \\ u_{Hall}B_y - v_{Hall}B_x \\ -(w_{Hall}B_x - u_{Hall}B_z) \\ 0 \end{bmatrix},$$

$$\mathbf{G}_{vis}(\mathbf{Q},\nabla\mathbf{Q}) = \begin{bmatrix} 0 \\ 0 \\ 0 \\ 0 \\ \|\mathbf{B}\|v_{Hall} - B_y(B_x u_{Hall} + B_y v_{Hall} + B_z w_{Hall}) \\ -(u_{Hall}B_y - v_{Hall}B_x) \\ 0 \\ v_{Hall}B_z - w_{Hall}B_y \\ 0 \end{bmatrix}. \tag{13}$$

The source term $\mathbf{M}$ is

$$\mathbf{M} = \begin{bmatrix} 0 \\ (\nabla \cdot \mathbf{B})B_x \\ (\nabla \cdot \mathbf{B})B_y \\ (\nabla \cdot \mathbf{B})B_z \\ (\nabla \cdot \mathbf{B})\mathbf{U} \cdot \mathbf{B} \\ (\nabla \cdot \mathbf{B})u \\ (\nabla \cdot \mathbf{B})v \\ (\nabla \cdot \mathbf{B})w \\ \alpha\psi \end{bmatrix}. \tag{14}$$

This code is two-dimensional ($\partial(\cdot)/\partial z \equiv 0$), though the time evolution of B_z and w are also computed.

3 Numerical Methods

The spectral difference divergence cleaning method is described at length by Chen & Liang (2022) in [7]. It is important to note that the Bassi & Rebay I [2] scheme is employed for the computation of the viscous fluxes, as this method is not compact and may be negatively affecting the stability of the spectral difference divergence cleaning method.

4 The GEM Magnetic Reconnection Challenge

The goal of the Geospace Environmental Modeling (GEM) Reconnection Challenge proposed by Birn & Drake in [3] is stated to be the identification of the essential physics which is required to model collisionless magnetic reconnection. Through their study, they found that models that include the Hall effect in the generalized Ohm's law produce very similar rates of reconnection, while the conventional resistive MHD model produces a dramatically smaller reconnection rate. Modern MHD codes are now tested using this problem with the goal of reproducing the results found in the paper. The SDDC code has been shown to produce a similar reconnection rate for the conventional resistive MHD equations, and is now being extended to the Hall MHD equations with the goal of producing faster reconnection.

4.1 Definition of the Problem

The domain is rectangular, where $-L_x/2 \leq x \leq L_x/2$ and $-L_y/2 \leq y \leq L_y/2$. The x direction is made periodic and ideal conducting boundaries are applied at $y = \pm L_y/2$, resulting in magnetic field boundary conditions of $B_y = \partial B_x/\partial y =$

$\partial B_z/\partial y = 0$ at the y boundaries, with corresponding conditions on the electric fields and fluid quantities.

The equilibrium magnetic field is given by

$$B_x(y) = B_0 tanh(y/\lambda), \tag{15}$$

and the density is given by

$$\rho(y) = \rho_0 sech^2(y/\lambda) + \rho_\infty. \tag{16}$$

Initially, the electron and ion temperatures, T_e and T_i, are taken to be uniform. This means that the pressure balance condition gives $\rho_0(T_e + T_i) = B_0^2/8\pi$.

The system is normalized to the Alfvén speed v_A, allowing B_0 and ρ_0 to both equal 1. Other specific parameters for the simulations are $\lambda = 0.5$, $\rho_\infty/\rho_0 = 0.2$, $T_e/T_i = 0.2$, $m_i/m_e = 25$, $L_x = 25.6$, and $L_y = 12.8$.

Grid spacing and resistivity are left open to be chosen specifically for each code. The simulations run in this paper use grids of 32x64 and 24x48 cells using a third and fourth order method respectively. We keep a consistent resistivity of $\eta = 0.005$, and we use a 5 stage 3rd order accurate Runge-Kutta time stepping scheme with a time step of $dt = 0.0001$ seconds.

The initial magnetic island is specified through the perturbation in the magnetic flux,

$$\psi(x, y) = \psi_0 cos(2\pi x/L_x) cos(\pi y/L_y), \tag{17}$$

where the magnetic field perturbation is given by $\mathbf{B} = \hat{z} \times \nabla\psi$. In normalized units $\psi_0 = 0.1$, producing an initial island width which is comparable to the initial width of the current layer.

4.2 Results

The speed of reconnection is visualized by plotting the reconnected flux over time. Reconnected flux can be calculated in slightly different ways, usually depending on if symmetry about the y axis is assumed. We calculate reconnected flux (ϕ) without assuming y axis symmetry by using the equation

$$\phi(t) = \frac{1}{2} \int_{-L_x/2}^{L_x/2} |B_y(x, y = 0, t)| dx. \tag{18}$$

It is important to note that all measures of time are in their nondimensionalized units and not in physical time.

In Fig. 2, the reconnected flux for the Hall MHD and conventional resistive MHD when using SDDC are plotted when a grid of 32x64 and a third-order method

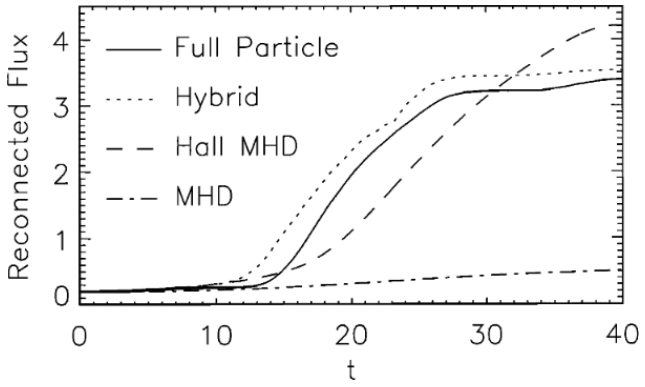

Figure 1: Reconnected flux reported in Birn & Drake et al. [3]. The "Full Particle" line shows the reconnected flux for a simulation that models everything as particles. The "Hybrid" line shows results of a model of nuclei and electrons as separate continuum. The "Two Fluid" line shows the result from using the Hall MHD system of equations. The "MHD" line shows the result from using the conventional resistive MHD equations.

is used. Figure 1 shows the reconnected flux obtained in Birn & Drake [3]. The reconnected flux produced by SDDC when using the resistive MHD equations shows that the simulation is no longer stable after 30 seconds. When using the Hall MHD equations, the reconnected flux shows that magnetic reconnection starts about 10 seconds later than expected. However, the shape of the reconnected flux plot for the Hall MHD equations produced by SDDC is similar to the shapes of the plots produced by Toth, Ma & Gombosi [14] and Birn & Drake et al. [3], suggesting that magnetic reconnection is happening as expected even though it is starting later.

In an effort to make the solver more stable for the resistive MHD equations and to get magnetic reconnection to start sooner, a new grid of 24x48 and a fourth-order method are used. Figure 3 shows the reconnected flux produced when using this grid, where it can be seen that the resistive MHD is more stable and magnetic reconnection begins only a few seconds later than expected. Compared to the results obtained when using SDDC on a 32x64 grid with a third-order SD method, the 24x48 grid with a fourth-order SD method gives results very similar to what was obtained in Toth, Ma & Gombosi [14] and Birn & Drake et al. [3]. The decrease in reconnected flux after about 36 seconds likely represents the merging of the central island with the larger island on the periodic boundaries.

Unfortunately, the GEM magnetic reconnection problem is very stiff when using the Hall MHD equations with SDDC, and no grid more fine than 24x48 and order of four can be used without decreasing the time step drastically, resulting in simulations that take an unreasonable amount of time.

The contours produced at various times are shown in Fig. 4 and 5 for a third

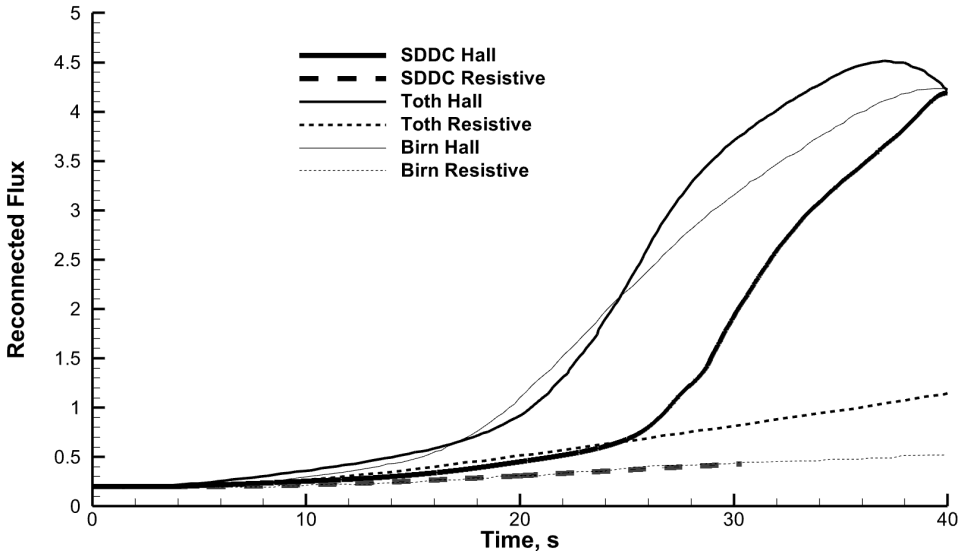

Figure 2: Reconnected flux plotted over 40 seconds for various equations. The lines labeled SDDC are the graphs produced in this work on a 32x64 grid using the third-order SD method. The lines labeled Toth show the data reported in Toth, Ma & Gombosi [14]. The lines labeled Birn show the data reported in Birn & Drake et al. [3].

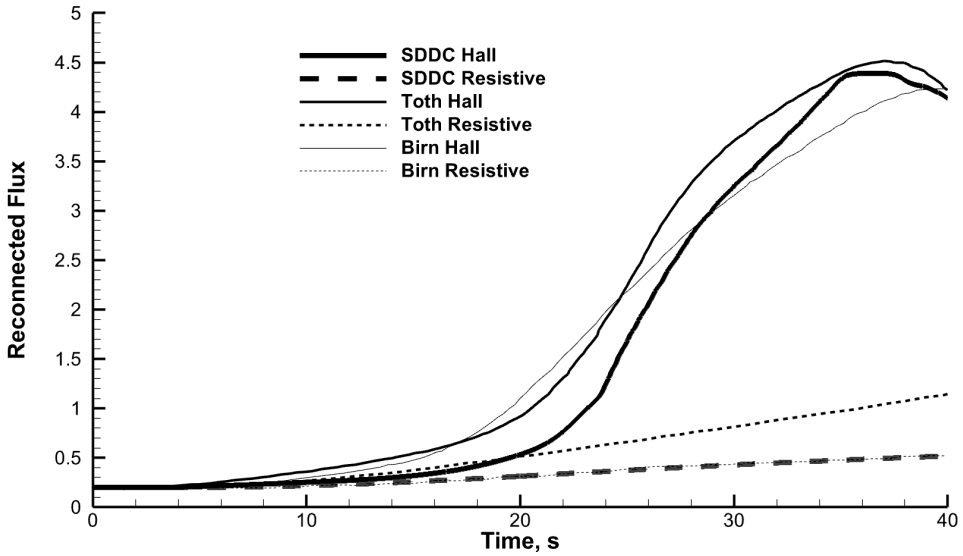

Figure 3: Reconnected flux plotted over 40 seconds for various equations. The lines labeled SDDC are the graphs produced in this work on a 24x48 grid using the fourth-order SD method. The lines labeled Toth show the data reported in Toth, Ma & Gombosi [14]. The lines labeled Birn show the data reported in Birn & Drake et al. [3].

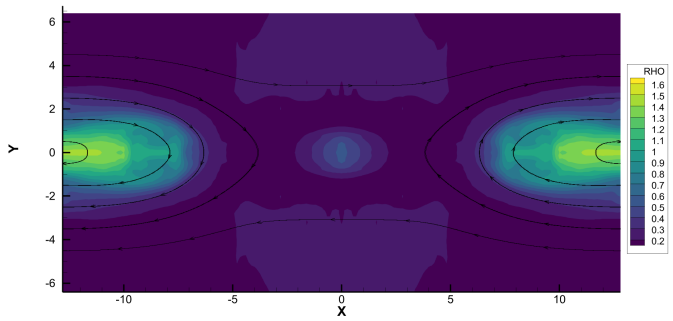

Figure 4: Density contour with magnetic field lines from a Hall MHD simulation at 50 seconds on a 32x64 grid using the third-order SD method.

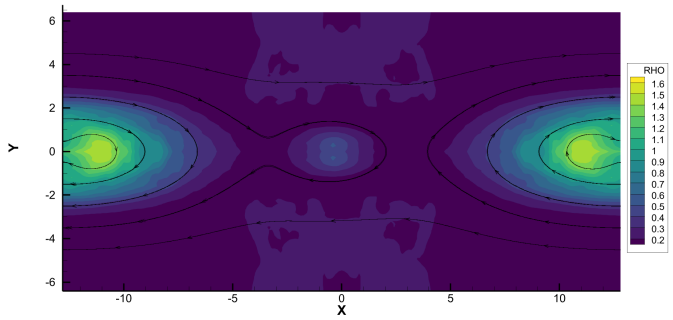

Figure 5: Density contour with magnetic field lines from a Hall MHD simulation at 70 seconds on a 32x64 grid using the third-order SD method.

order simulation on a 32x64 grid when using the Hall MHD equations. Figures 6, 7 and 8 show contours produced using a fourth order simulation on a 24x48 grid for the Hall MHD equations. The contour at 70 seconds using the 32x64 grid (Figure 5) shows that the central island starts moving to the left to merge with the larger island. Similarly, when using the 24x48 grid the same behavior can be seen (Fig. 7), though it happens faster with the central island moving at around 42 seconds. Ideally, a finer grid would have been used to observe the movement of the central island because it is expected to be stationary when using the Hall MHD equations.

When using the resistive MHD equations for the 24x48 grid setup, the contours shown in Fig. 9, 10 and 11 are produced. As expected, the simulation takes longer to show the formation of islands compared to when the Hall MHD equations are used, though again the use of a finer grid would have been ideal. This is because the resistive MHD equations are still expected to produce a central island, which is

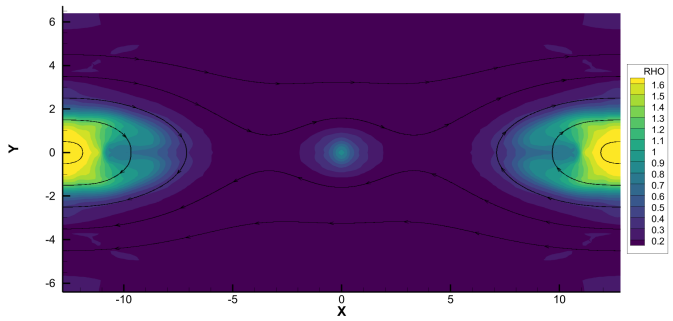

Figure 6: Density contour with magnetic field lines from a Hall MHD simulation at 30 seconds on a 24x48 grid using the fourth-order SD method.

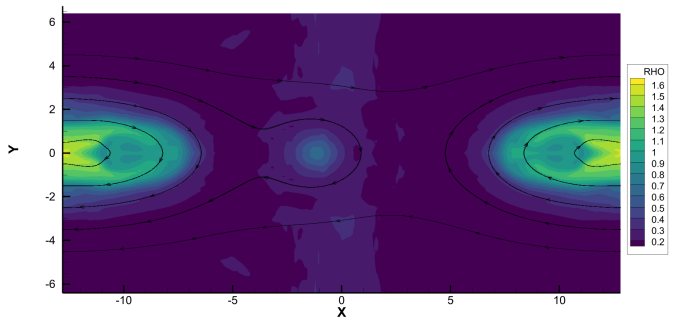

Figure 7: Density contour with magnetic field lines from a Hall MHD simulation at 42.5 seconds on a 24x48 grid using the fourth-order SD method.

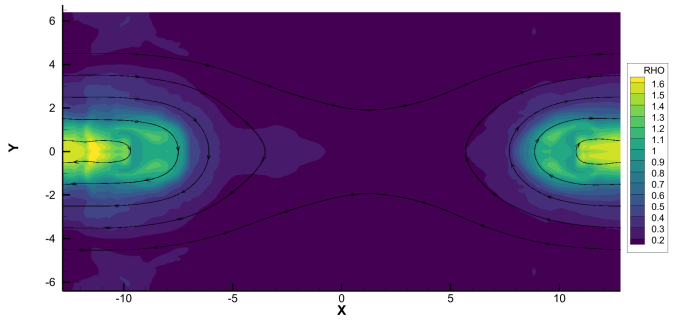

Figure 8: Density contour with magnetic field lines from a Hall MHD simulation at 50 seconds on a 24x48 grid using the fourth-order SD method.

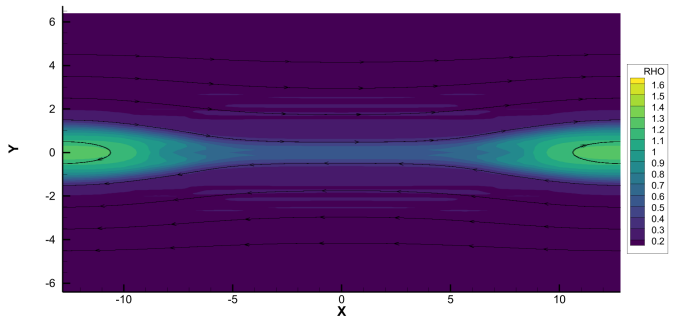

Figure 9: Density contour with magnetic field lines from a Resistive MHD simulation at 30 seconds on a 24x48 grid using the fourth-order SD method.

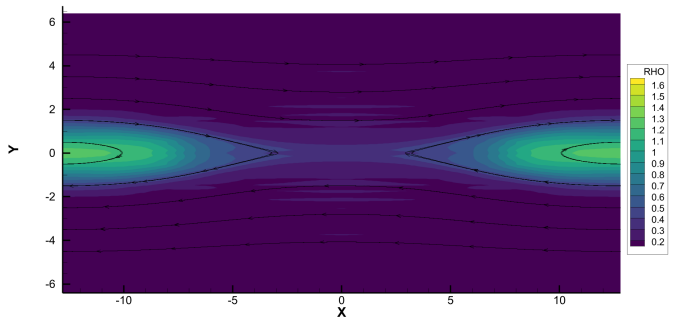

Figure 10: Density contour with magnetic field lines from a Resistive MHD simulation at 50 seconds on a 24x48 grid using the fourth-order SD method.

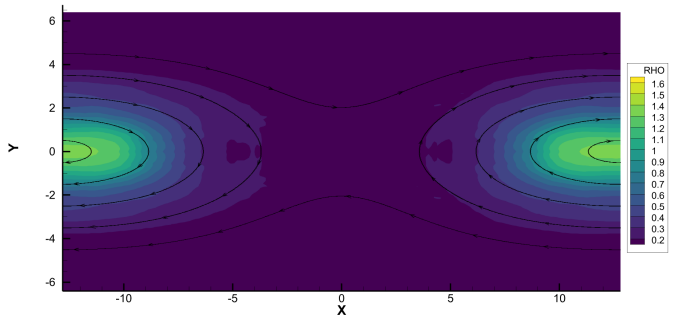

Figure 11: Density contour with magnetic field lines from a Resistive MHD simulation at 200 seconds on a 24x48 grid using the fourth-order SD method.

not seen at any point when using the 24x48 grid setup. However, through analysis of the animation produced, it can be seen that the density contour fluctuates in a manner that suggests a central island was present and moved to the right, but that the grid was too coarse to show its formation.

5 Future Work

In future works, attempts will be made to increase the resolution of the grid without losing simulation stability. Success in refining the grid is expected to cause reconnection to begin sooner in the Hall MHD simulation. Additionally, it is expected that the type of numerical flux between cells has a large effect on stability, suggesting that future work which switches the current Rusanov flux with a different solver will be worthwhile.

Future works will also involve modification of the Spectral Difference Constrained Transport (SDCT) code produced by Chen & Liang 2022 in [6] which preserves the $\nabla \cdot \mathbf{B} = 0$ condition exactly. It is expected that more stable simulations will be produced because of this property, allowing for the use of finer grids.

Acknowledgments

The research work of all authors has been supported by a National Science Foundation (NSF) CAREER award (No. 1952554) to PI Liang and an Air Force Office of Scientific Research (AFOSR) grant (award No. FA9550-20-1-0374) monitored by Dr. Fariba Fahroo. Undergraduate research assistant, Russell Hankey, was also supported by the REU program funded through an NSF award No. 1852102 at Clarkson University.

References

[1] Dinshaw S Balsara and Daniel S Spicer. A Staggered Mesh Algorithm Using High Order Godunov Fluxes to Ensure Solenoidal Magnetic Fields in Magnetohydrodynamic Simulations. *Journal of Computational Physics*, 149(2):270–292, 1999.

[2] F. Bassi and S. Rebay. A high-order accurate discontinuous finite element method for the numerical solution of the compressible Navier-Stokes equations. *Journal of Computational Physics*, 131:267–279, 1997.

[3] J. Birn, J. F. Drake, M. A. Shay, B. N. Rogers, R. E. Denton, M. Hesse, M. Kuznetsova, Z. W. Ma, A. Bhattacharjee, A. Otto, and P. L. Pritch-

ett. Geospace Environmental Modeling (GEM) Magnetic Reconnection Challenge. *Journal of Geophysical Research: Space Physics*, 106(A3):3715–3719, 2001.

[4] M. Bohm, A. R. Winters, G. J. Gassner, D. Derigs, F. Hindenlang, and J. Saur. An entropy stable nodal discontinuous galerkin method for the resistive MHD equations. Part I: Theory and numerical verification. *Journal of Computational Physics*, 422:108076, 2020.

[5] J.U Brackbill and D.C Barnes. The Effect of Nonzero $\nabla \cdot \mathbf{B}$ on the numerical solution of the magnetohydrodynamic equations. *Journal of Computational Physics*, 35(3):426–430, 1980.

[6] Kuangxu Chen and Chunlei Liang. A Divergence-Free High-Order Spectral Difference Method with Constrained Transport for Ideal Compressible Magnetohydrodynamics. *International Journal of Computational Fluid Dynamics*, 35(10):826–849, 2021.

[7] Kuangxu Chen and Chunlei Liang. An Arbitrarily High-order Spectral Difference Method with Divergence Cleaning (SDDC) for Compressible Magnetohydrodynamic Simulations on Unstructured Grids. *The Astrophysical Journal*, 932(1):16, jun 2022.

[8] Bernardo Cockburn, Fengyan Li, and Chi-Wang Shu. Locally divergence-free discontinuous Galerkin methods for the Maxwell equations. *Journal of Computational Physics*, 194(2):588–610, 2004.

[9] A. Dedner, F. Kemm, D. Kröner, C.-D. Munz, T. Schnitzer, and M. Wesenberg. Hyperbolic Divergence Cleaning for the MHD Equations. *Journal of Computational Physics*, 175(2):645–673, 2002.

[10] Dominik Derigs, Andrew R. Winters, Gregor J. Gassner, Stefanie Walch, and Marvin Bohm. Ideal GLM-MHD: About the entropy consistent nine-wave magnetic field divergence diminishing ideal magnetohydrodynamics equations. *Journal of Computational Physics*, 364:420–467, 2018.

[11] Charles R. Evans and John F. Hawley. Simulation of Magnetohydrodynamic Flows: A Constrained Transport Model. , 332:659, September 1988.

[12] Kenneth G. Powell, Philip L. Roe, Timur J. Linde, Tamas I. Gombosi, and Darren L. De Zeeuw. A Solution-Adaptive Upwind Scheme for Ideal Magnetohydrodynamics. *Journal of Computational Physics*, 154(2):284–309, 1999.

[13] Gábor Tóth. The $\nabla \cdot \mathbf{B} = 0$ Constraint in Shock-Capturing Magnetohydrodynamics Codes. *Journal of Computational Physics*, 161(2):605–652, 2000.

[14] Gábor Tóth, Yingjuan Ma, and Tamas I. Gombosi. Hall magnetohydrodynamics on block-adaptive grids. *Journal of Computational Physics*, 227(14):6967–6984, 2008.

[15] Yun Yang and Ward B. Manchester IV. Using a Higher-order Numerical Scheme to Study the Hall Magnetic Reconnection. *The Astrophysical Journal*, 892(1):61, mar 2020.

[16] Andrew L. Zachary, Andrea Malagoli, and Phillip Colella. A Higher-Order Godunov Method for Multidimensional Ideal Magnetohydrodynamics. *SIAM Journal on Scientific Computing*, 15(2):263–284, 1994.